Exploration of a Remote Antineutrino-Based Monitoring Concept for Small Modular Reactors

Emma Houston[1]

Adam Bernstein[2]

Tomi Akindele[3]

Marc Bergevin[4]

Sandra Bogetic[5]

University of Tennessee, Knoxville, TN 37902

Abstract

Neutrino detectors have been proposed to meet the safeguards challenges for the next generation of nuclear reactors [1], [2]. While small modular reactors offer some nonproliferation benefit arising from their smaller source terms and (frequently) sealed designs, the prospect of remote and widespread deployment may introduce new challenges for next-generation nuclear reactor safeguards [3]. Neutrino detection experiments have shown the ability to monitor reactor power from distances beyond the reactor site perimeter [4–7]. In this study we describe a possible method for identifying a cost-effective detector design with minimal mass and overburden, while ensuring collection of sufficient antineutrino data to detect potential diversion.

[1]E-mail:ehoust10@vols.utk.edu
[2]E-mail:bernstein3@llnl.gov
[3]E-mail:akindele1@llnl.gov
[4]E-mail:bergevin1@llnl.gov
[5]E-mail:sbogetic@utk.edu

1 Introduction to Neutrino Detectors

The last few decades of neutrino detector operations have demonstrated successful power and fuel burnup monitoring at reactors sites. Power monitoring can provide a continuity of knowledge at nuclear reactors, and can both deter and detect potential diversion [8]. Due to the small interaction cross sections, neutrinos can travel far distances and remain undetected. Thus, they cannot be shielded, unlike other radiation signatures from nuclear fuel. The unshieldable nature of the antineutrino and the ability to be detected at a significant distance away from the reactor core offers some advantages compared to current safeguards approaches [2].

Neutrino[6] detectors often rely on inverse beta decay (IBD) reactions, in proton-rich hydrogenous materials. In the IBD process, antineutrinos interact with a free proton and produce a positron and neutron pair [9]. The threshold energy for this interaction is 1.8 MeV [9]. The positron is detected first. The neutron thermalizes in the detector volume and is captured a few tens or hundreds of microseconds later by hydrogen or a doping agent such as gadolinium [8].

$$\bar{\nu}_e + p \longrightarrow e^+ + n \tag{1}$$

Many currently proposed advanced reactors are designed to have significantly smaller footprints than the current generation of light water reactors. The emergency planning zone and low population zone requirements are determined, in part, by the reactor source terms [10]. For small modular reactors (SMRs) these source terms are significantly smaller and thus these sites have a smaller footprint. This smaller footprint makes SMRs potentially attractive for neutrino detectors to be used as a safeguards tool, since the detector could remain outside of the site perimeter and still collect an adequate signal on timescales consistent with current IAEA timeliness goals for Pressurized Water Reactors (PWR) and other current reactor designs. The goal of this study is to identify the smallest and shallowest detector that can remain outside of the exclusion area of a reactor site, and have a large enough signal to maintain the timeliness detection goals and missed and false alarm requirements imposed by the IAEA that prevail for existing reactors.

The focus of our study is the NuScale SMR site design [11]. The design contains multiple cores, all operating at 160 MWth, within a common containment structure. Fuel bundles are in 17 by 17 arrays, similar to those found in the current fleet of light water reactors [12]. While this fuel type itself doesn't pose challenges to the current safeguard regime, the remoteness and the sheer number of proposed small modular reactors to be deployed poses significant potential burden on the ability to safeguard these reactors [3]. Increased deployment was listed as one of the most challenging nonproliferation aspects of SMRs [3]. There is a significant cost associated with the size of detectors and thus the goal is to be able to minimize the detector size in order to identify an affordable option for reactor monitoring. Fig. 1 shows a site map that we have used to approximate the distance from the reactor to the perimeter of the site. This is considered the minimum distance for the proposed neutrino detector [11].

---

[6]In keeping with common practice, we may use the shorthand term 'neutrino detector' to refer to devices which detect antineutrinos. In the case of reactors the signal consists of uniquely of antineutrinos.
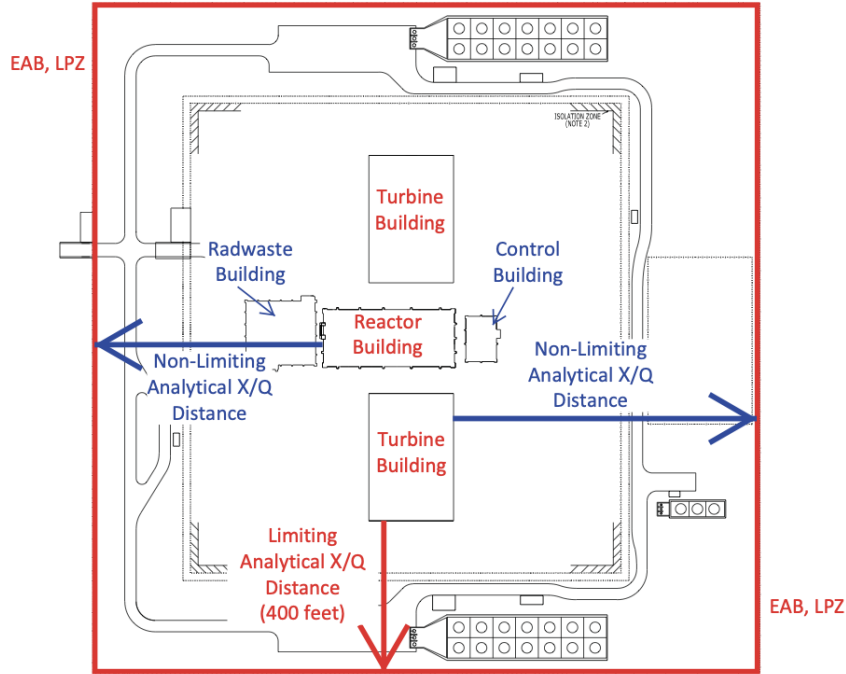
Figure 1: Above is the site map of the NuScale site used to approximate the distance from the reactor to the site perimeter. This is considered the shortest distance the detector can be to remain non-intrusive. [11]

2 Diversion Scenario

To simulate the effectiveness of a neutrino detector as a safeguards tool, its efficacy was tested against potential diversion scenarios. Through the cycle, neutron capture on ^{238}U leads to the production of ^{239}Pu. However, further into the cycle, other isotopes of Plutonium, including ^{240}Pu and ^{241}Pu, are produced and the desirable ratio of ^{239}Pu to a proliferator deteriorates through the cycle. Thus, one potential diversion scenario is to operate all cores at a lower power to improve the ^{239}Pu ratio. Another potential diversion scenario is the premature removal of fuel prior to scheduled outages. This would cause the complete shutdown in one of the six cores within containment. Both of these scenarios share the common feature of a reduction in power indicative of anomalous and possibly proscribed activity. Since the antineutrino signal is proportional to the reactor thermal power, such an anomalous power can be observed by measuring the antineutrino signal continuously over periods of weeks to months. While these scenarios are illustrative, they are not exhaustive, and there are likely other scenarios, such as power increases, which may also be detectable via the antineutrino signature.

3 Method

3.1 Signal

The following equations shows the equation to approximate signal rates [8].

$$N_{det}(E_\nu, t) = \frac{\epsilon(E_\nu)}{4\pi L^2} \phi_\nu(E_\nu, t) \sigma(E_\nu) N_T P_{surv}(E_\nu, L) \qquad (2)$$

In Eq. 2 above, ϵ is the energy-dependent efficiency of the spectra. For simplicity, this number is assumed to be 80% based on previous neutrino detector experiments [5], [13]. L is the distance from the reactor to the detector. In the case of NuScale, this was approximated to be 800 feet, or 244 m, based on Fig. 1, from NuScale application documentation [11]. The energy and time-dependent emitted antineutrino flux (in units of antineutrinos per fission per MeV), is represented by $\phi_\nu(E_\nu, t)$. This is given by the fifth order polynomial for energy-dependent neutrino flux [14], [15]. The fuel composition and energy per fission used in this study are given in the Table III of the following reference [16]. The neutrino survival probability is represented as P_{surv} and given by the Equation 65.9 in the following reference [17]. The cross-section, σ, is calculated for all neutrino emission energies [18]. The target number of protons in the volume is dependent on the mass of detector. The density of linear alkylbenzene is 0.86 g/cm^3 and there are 30 free protons per molecule [19]. Using these values the total number of free target protons per ton is 7.5×10^{28} free protons/ton. For varying size detectors, this number is scaled to find the total number of target protons in each detector. Lastly, the systematic uncertainty of the signal is estimated to be 5.25%. The Double Chooz experiment reported a systematic uncertainty of 1.7% [5], however to provide a conservative estimate, it is assumed that the reactor power uncertainty has increased from 0.5% to 5%.

Using the theoretical antineutrino signal rates calculated for the NuScale SMR, and accounting for signal and background rates and detection efficiencies, we can estimate the time to detect a decrease in power arising from one of the aforementioned diversion scenarios.

3.2 Backgrounds

The backgrounds considered in this study were Li-He production, fast neutrons, and accidental backgrounds. ^{9}Li and ^{8}He, both proceed through a β decay and subsequent neutron decay, which combination of interactions mimics the IBD signature. These unstable, neutron-rich radionuclides are induced by cosmogenic muons interacting with ^{12}C in the scintillator volume [20, 21]. Cosmogenic muons interacting with the rock surrounding the detector may additionally cause fast neutrons to enter the detector and mimic the coincidence requirements of an IBD reaction [18]. These fast neutrons may create a pair of time-correlated signals that meets the time coincidence and energy deposition criteria for the inverse beta decay antineutrino backgrounds, thus comprising our second type of background.

Previous detector experiments have measured both cosmogenically induced backgrounds and are shown in Table 1. Using data form these experiments, a scaling metric for both of these background types has been created. Fast neutrons interact with the rock surrounding the detector, and thus scale with the surface area of the detector. On the other hand, Li-He backgrounds scale with the volume of the detector.
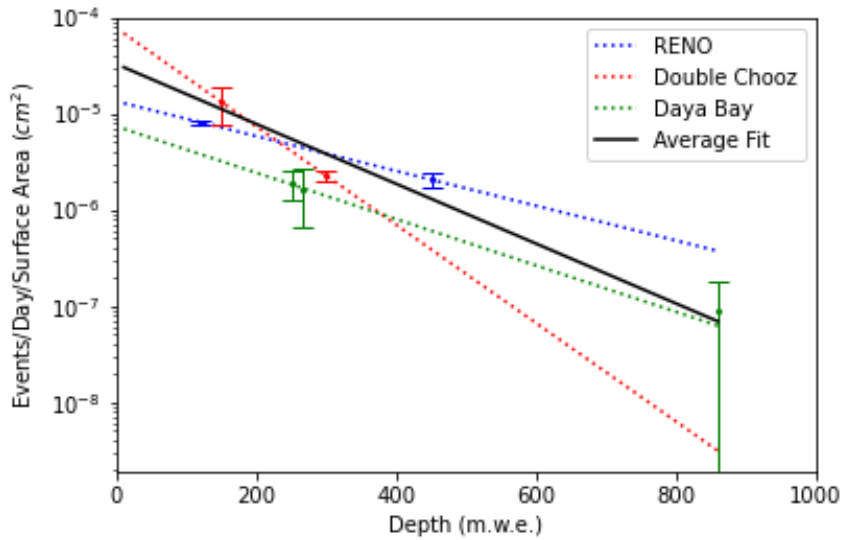
Figure 2: shows the fast neutron background rate from previous detector experiments. The average fit is shown in black and used to predict fast neutron backgrounds at shallower depths.
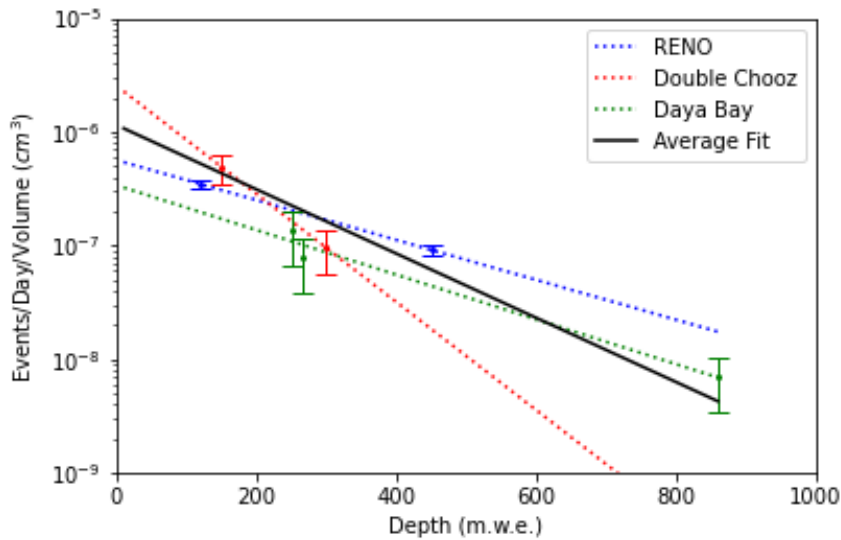

Figure 3: shows the Li-He background rate from previous detector experiments. The average fit is shown in black and used to predict Li-He production backgrounds at shallower depths.

Using these extrapolated functions, the backgrounds for Li-He and fast neutrons were approximated based on the depth of the detector. Accidental backgrounds are caused by a number of factors, including radioactive impurities present throughout the detector volume, in photosensors, and in structural materials, the composition of the surrounding rock, detector cleanliness procedures, and other factors. This makes it difficult to predict the accidentals rate within

4

the detector. The largest accidentals rate with respect to the surface area of the detector is found to be $5.57 \times 10^{-5} \frac{events}{day-cm^2}$. Additionally, the largest relative uncertainty is used in order to generate the uncertainty in each of the extrapolated backgrounds. Generally, this will tend to over-estimate the systematic uncertainty in each of these backgrounds, a conservative choice.

Table 1: shows the background data from Li-He, fast-neutrons, and accidentals to create the functions to predict background contributions from each muogenic background type.

Experiment	Depth m.w.e.	Li-He events/day	Fast Neutrons events/day	Accidentals events/day
RENO	120	12.45 ± 5.93 [22]	5.0 ± 0.13 [22]	4.3 ± 0.06 [23]
Double Chooz	150	5.01 ± 1.43[24]	3.42 ± 0.23 [24]	0.344 ± 0.002 [24]
Daya Bay	250	3.1 ± 1.6 [13]	0.84 ± 0.28 [13]	9.85 ± 0.06 [22]
Daya Bay	265	1.8 ± 1.1 [13]	0.74 ± 0.44 [13]	7.67 ± 0.05 [22]
Double Chooz	300	$0.97^{+0.41}_{-0.16}$ [24]	0.586 ± 0.061 [24]	0.106 ± 0.002 [24]
RENO	450	2.59 ± 0.75 [22]	0.97 ± 0.06 [22]	0.68 ± 0.03 [23]
Daya Bay	860	0.16 ± 0.11 [13]	0.04 ± 0.04 [13]	3.25 ± 0.03 [22]

3.3 Data Generation

Each of the diversion scenarios is dependent on the ability to see a decrease in signal, which would be indicative of a decrease in reactor power. In order to simulate potential detector data from an operating reactor, the numpy random sampling feature is used [25]. To simulate normal operation (6 operating cores) the signal rates are randomly sampled from a Guassian function. Another case is simulated with all of the cores operating per declarations at 100% for the first 100 days, followed by 5 of the 6 cores operating at full power, for the second 100 days. The latter case simulates both of our diversion scenarios.

4 Results

Fig. 4 shows the sampled data for both cases, diversion and no diversion for a 3 ton detector at 20 mwe underground. The black horizontal lines indicate the number of sigma from the expected values of detectors response for 6 cores operating. Fig. 4 demonstrates the difficulty differentiating between 5 and 6 cores operating. For a clearer differentiation between the two operational states, a rolling aggregate count of data is taken over several days. This rolling aggregate is then subtracted from the expected number of events over the same time period. For declared operations, the subtracted quantity will fluctuate about zero with a sigma determined by the aggregate counts in the defined time interval (i.e., the event rate per day multiplied by the integration time in days). With this subtraction, systematic uncertainties are largely removed, so that fluctuations are predominantly statistical. Fig. 5 shows this quantity plotted against time in days.

From Fig. 5, the difference between the expected events and aggregate counts for a 10 day time window, is more clearly seen. When this difference crosses a 3-sigma threshold, this is registered as the time in which detection of potential diversion occurred. This example shows one randomly sampled data set and the associated detection time for the power anomaly. The
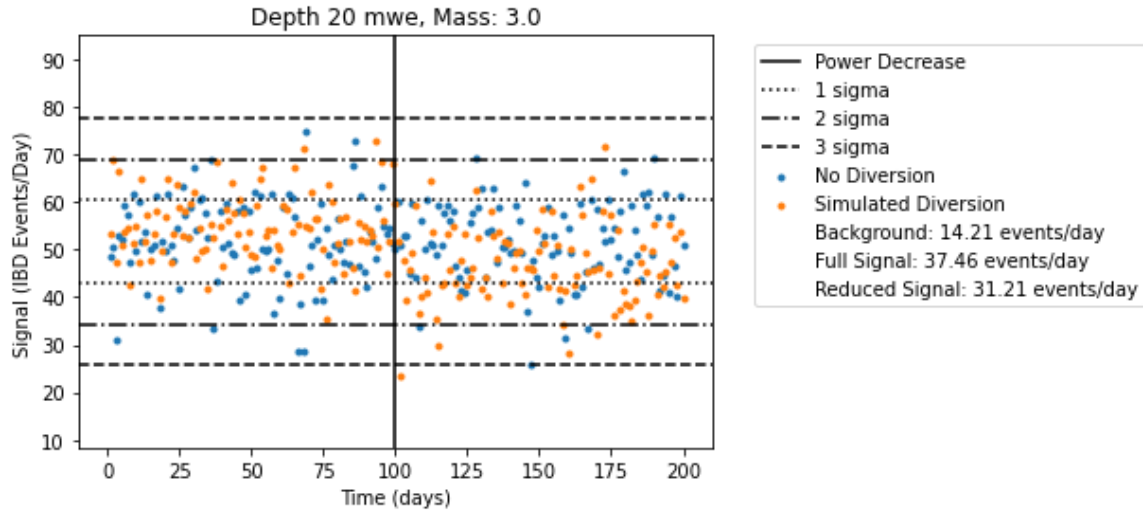
Figure 4: shows the gaussian distributed counts for both a diversion and non-diversion scenario.
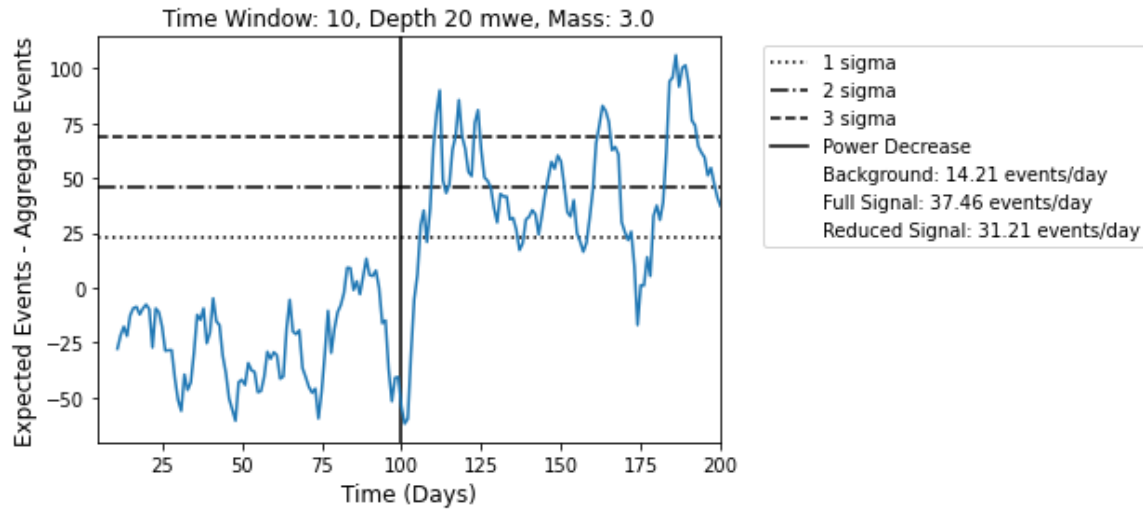

Figure 5: shows the time aggregate counts subtracted from the expected counts over a 10 day time window. The solid vertical line indicates the time of diversion.

average time-to-detect for the anomalous power excursion is calculated by sampling multiple randomly generated data sets with the same underlying power-versus-time profile.

If this difference crosses the 3-sigma threshold prior to a simulated change in reactor power, this is considered a false alarm. Dependent on the state requirements, set by the IAEA, the missed alarms can be identified as instances in which the time taken to detect diversion surpasses the timeliness detection goal.

5   Conclusions and Ongoing Work

This method shows a process by which neutrino detectors can potentially be utilized as a safeguards tool at SMR sites, specifically the NuScale SMR. In a forthcoming publication, we will use the process described above (repeated for a large set of randomly sampled antineutrino count rate evolutions) to identify a combination of detector size and depth that can meet the IAEA timeliness detection goals while remaining cost-effective. Additionally, an assessment of the state may drive the allowable false and missed alarm rates along with the timeliness detection requirements.

References

[1] Proceedings of the first meeting of the ad hoc working group on safeguards applications utilizing antineutrino detection and monitoring. Technical report, 2011.

[2] Christopher Stewart, Abdalla Abou-Jaoude, and Anna Erickson. Employing antineutrino detectors to safeguard future nuclear reactors from diversions. *Nature communications*, 10(1):3527, 2019.

[3] Shikha Prasad, Ahmed Abdulla, M Granger Morgan, and Inés Lima Azevedo. Nonproliferation improvements and challenges presented by small modular reactors. *Progress in Nuclear Energy*, 80:102–109, 2015.

[4] F. Boehm, J. Busenitz, B. Cook, G. Gratta, H. Henrikson, J. Kornis, D. Lawrence, K. B. Lee, K. McKinny, L. Miller, V. Novikov, A. Piepke, B. Ritchie, D. Tracy, P. Vogel, Y-F. Wang, and J. Wolf. Results from the palo verde neutrino oscillation experiment. *Phys. Rev. D*, 62:072002, Sep 2000.

[5] Rachel Carr. *Measurements of Electron Antineutrino Disappearance in the Double Chooz Experiment*. Columbia University, 2015.

[6] RENO Collaboration and J. K. Ahn. Reno: An experiment for neutrino oscillation parameter θ_{13} using reactor neutrinos at yonggwang, 2010.

[7] Jun Cao and Kam-Biu Luk. An overview of the daya bay reactor neutrino experiment. *Nuclear Physics B*, 908:62–73, 2016.

[8] Adam Bernstein, Nathaniel Bowden, Bethany L Goldblum, Patrick Huber, Igor Jovanovic, and John Mattingly. Colloquium: Neutrino detectors as tools for nuclear security. *Reviews of Modern Physics*, 92(1):011003, 2020.

[9] Patrick Huber. Reactor antineutrino fluxes–status and challenges. *Nuclear Physics B*, 908:268–278, 2016.

[10] Nuclear Regulatory Commission (NRC). Methods and assumptions for evaluating radiological consequences of design basis accidents at light-water nuclear power reactors. Technical report, 2003.

[11] NuScale. Nuscale standard plant design certification application: Site characteristics and site parameters. https://www.nrc.gov/docs/ML2022/ML20224A482.pdf, 2020.

[12] NuScale. Nuscale standard plant design certification application: Reactor. https://www.nrc.gov/docs/ML2022/ML20224A482.pdf, 2020.

[13] FP An, JZ Bai, AB Balantekin, HR Band, D Beavis, W Beriguete, M Bishai, S Blyth, K Boddy, RL Brown, et al. Observation of electron-antineutrino disappearance at daya bay. *Physical Review Letters*, 108(17):171803, 2012.

[14] Patrick Huber. Determination of antineutrino spectra from nuclear reactors. *Physical Review C*, 84(2):024617, 2011.

[15] Th A Mueller, D Lhuillier, Muriel Fallot, A Letourneau, S Cormon, M Fechner, Lydie Giot, Th Lasserre, J Martino, G Mention, et al. Improved predictions of reactor antineutrino spectra. *Physical Review C*, 83(5):054615, 2011.

[16] Viacheslav A Li, Steven A Dazeley, Marc Bergevin, and Adam Bernstein. Scalability of gadolinium-doped-water cherenkov detectors for nuclear nonproliferation. *Physical Review Applied*, 18(3):034059, 2022.

[17] Particle Data Group. Review of particle physics. *Phys. Rev. D*, 98:030001, Aug 2018.

[18] Y Abe, Christoph Aberle, JC Dos Anjos, JC Barriere, M Bergevin, A Bernstein, TJC Bezerra, L Bezrukhov, E Blucher, NS Bowden, et al. Reactor ν e disappearance in the double chooz experiment. *Physical Review D*, 86(5):052008, 2012.

[19] Minfang Yeh, A Garnov, and Richard L Hahn. Gadolinium-loaded liquid scintillator for high-precision measurements of antineutrino oscillations and the mixing angle, $\theta 13$. *Nuclear Instruments and Methods in Physics Research Section A: Accelerators, Spectrometers, Detectors and Associated Equipment*, 578(1):329–339, 2007.

[20] Jun Cao and Kam-Biu Luk. An overview of the daya bay reactor neutrino experiment. *Nuclear Physics B*, 908:62–73, 2016. Neutrino Oscillations: Celebrating the Nobel Prize in Physics 2015.

[21] Cara Nichole Maesano. *Lithium-9 Production from Stopped Muons in the Double Chooz Detector*. University of California, Davis, 2012.

[22] Jung Keun Ahn, S Chebotaryov, JH Choi, S Choi, W Choi, Y Choi, HI Jang, JS Jang, EJ Jeon, IS Jeong, et al. Observation of reactor electron antineutrinos disappearance in the reno experiment. *Physical Review Letters*, 108(19):191802, 2012.

[23] J. K. Ahn, S. Chebotaryov, J. H. Choi, S. Choi, W. Choi, Y. Choi, H. I. Jang, J. S. Jang, E. J. Jeon, I. S. Jeong, K. K. Joo, B. R. Kim, B. C. Kim, H. S. Kim, J. Y. Kim, S. B. Kim, S. H. Kim, S. Y. Kim, W. Kim, Y. D. Kim, J. Lee, J. K. Lee, I. T. Lim, K. J. Ma, M. Y. Pac, I. G. Park, J. S. Park, K. S. Park, J. W. Shin, K. Siyeon, B. S. Yang, I. S. Yeo, S. H. Yi, and I. Yu. Observation of reactor electron antineutrinos disappearance in the reno experiment. *Phys. Rev. Lett.*, 108:191802, May 2012.

[24] Stefan Schoppmann, Double-Chooz Collaboration, et al. Latest results of double chooz. In *XIII International Conference on Heavy Quarks and Leptons*, volume 274, page 010. SISSA Medialab, 2017.

[25] Charles R. Harris, K. Jarrod Millman, Stéfan J. van der Walt, Ralf Gommers, Pauli Virtanen, David Cournapeau, Eric Wieser, Julian Taylor, Sebastian Berg, Nathaniel J. Smith, Robert Kern, Matti Picus, Stephan Hoyer, Marten H. van Kerkwijk, Matthew Brett, Allan Haldane, Jaime Fernández del Río, Mark Wiebe, Pearu Peterson, Pierre Gérard-Marchant, Kevin Sheppard, Tyler Reddy, Warren Weckesser, Hameer Abbasi, Christoph Gohlke, and Travis E. Oliphant. Array programming with NumPy. *Nature*, 585(7825):357–362, September 2020.